



## Chemically tailored high- $\chi$ block copolymers for perpendicular lamellae via thermal annealing

Journal:	<i>Soft Matter</i>
Manuscript ID	SM-ART-01-2019-000128.R1
Article Type:	Paper
Date Submitted by the Author:	22-Feb-2019
Complete List of Authors:	Yoshimura, Yasunari; Tokyo Institute of Technology, Department of Materials Science and Engineering, School of Materials and Chemical Technology Chandra, Alvin; Tokyo Institute of Technology, Department of Materials Science and Engineering, School of Materials and Chemical Technology Nabae, Yuta; Tokyo Institute of Technology, Department of Materials Science and Engineering, School of Materials and Chemical Technology Hayakawa, Teruaki ; Tokyo Institute of Technology, Department of Materials Science and Engineering, School of Materials and Chemical Technology



Journal Name

ARTICLE

## Chemically tailored high- $\chi$ block copolymers for perpendicular lamellae via thermal annealing

Yasunari Yoshimura, Alvin Chandra, Yuta Nabae and Teruaki Hayakawa\*

Received 00th January 20xx,  
Accepted 00th January 20xx

DOI: 10.1039/x0xx00000x

www.rsc.org/

A chemically tailored high- $\chi$  block copolymer (BCP), polystyrene-*block*-poly[2-hydroxy-3-(2,2,2-trifluoroethylsulfanyl)propyl methacrylate] (PS-*b*-PHFMA), was designed to incorporate tailored surface affinities and chemical incompatibilities for engineering perpendicular lamellae using thermal annealing. PS-*b*-PHFMA was synthesized via the sequential anionic polymerization of styrene and glycidyl methacrylate and the post-polymerization functionalization of the glycidyl moieties with 2,2,2-trifluoroethanethiol. The bulk studies revealed lamellae with a minimum domain spacing of 9.6 nm and a large effective Flory–Huggins interaction parameter ( $\chi_{\text{eff}}$ ) of 0.191 at 25 °C. Furthermore, atomic force microscopy and scanning electron microscopy showed perpendicular lamellae of the PS-*b*-PHFMA prepared on thermally-annealed thin films. The introduction of hydrophobic trifluoroethyl moieties onto the hydrophilic glycidyl moieties successfully balanced the surface affinity of the PHFMA block relative to PS, while simultaneously increasing the strength of segregation. Thus,  $\chi_{\text{eff}}$  of the chemically tailored BCP increased, and a perpendicular orientation was facilitated on the thin films using thermal annealing.

### Introduction

In the past few decades, block copolymer (BCP) lithography has received increasing attention as a potential next generation lithographic process for the semiconductor industry.<sup>1,2</sup> The 5–300-nm scale nanoassemblies of BCPs<sup>3,4</sup> can be used as resists for transferring patterns onto any underlying substrate. By engineering perpendicular lamellar structures from strongly segregating high- $\chi$  BCPs on thin films, line and space (L/S) structures with feature sizes less than 5 nm can be obtained.<sup>3,5–12</sup> However, the development of high- $\chi$  BCPs that can form perpendicular structures on thin films is challenging.

Typically, high- $\chi$  BCP systems pair largely chemically disparate polymers, such as hydrophobic-hydrophilic or organic-inorganic BCPs,<sup>3,5–22</sup> resulting in the selective segregation of one segment and the formation of parallel structures. To overcome this issue, several processes, such as precisely controlling the annealing process<sup>5,7,13,15,23</sup> and introducing chemically-modified interfaces,<sup>9,18,24–26</sup> have been developed to achieve a perpendicular orientation of the high- $\chi$  BCP thin films. Conversely, Kim et al. proposed a BCP design concept that contained polymer segments with well-balanced affinities

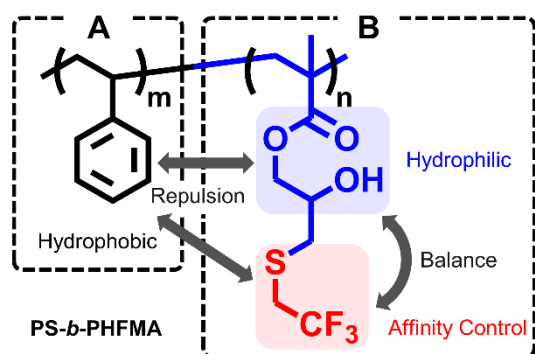
toward the air interface, facilitating a perpendicular orientation by thermal annealing.<sup>27</sup> Subsequently, increased efforts have been dedicated to develop high- $\chi$  BCPs that form a perpendicular structure via only thermal annealing.<sup>16,20–22,28–30</sup> Similarly, polystyrene-*block*-poly(methyl methacrylate) (PS-*b*-PMMA) has been the most studied BCP for lithographic applications owing to their ability to form perpendicular structures, while requiring only facile thermal annealing in thin films on surface neutralized substrates.<sup>31,32</sup> However, because of the low effective Flory–Huggins interaction parameter ( $\chi_{\text{eff}}$ ),<sup>33,34</sup> PS-*b*-PMMA has disadvantages, such as a limited minimum feature size,<sup>35</sup> for next-generation lithographic material applications.

Therefore, a novel concept was proposed for the design of chemically tailored high- $\chi$  BCPs based on polystyrene-*block*-polymethacrylate that is capable of forming perpendicular structures on thin films by thermal annealing, as shown in Scheme 1. In high- $\chi$  BCPs consisting of a hydrophobic A block and a hydrophilic B block on neutral substrates, the A block segregates to the free surface, resulting in a parallel orientation. To resolve this issue, the proposed design functionalizes the hydrophilic B block with distinctly hydrophobic units. This affinity control unit can be used to tailor the affinity of the B block against the free surface owing to its hydrophobic nature, while strengthening the chemical incompatibility between the A and B segments.

Based on this concept, polystyrene-*block*-poly(glycidyl methacrylate) (PS-*b*-PGMA) was synthesized, and a trifluoroethyl-containing affinity control unit was introduced to

\* Department of Materials Science and Engineering, School of Materials and Chemical Technology, Tokyo Institute of Technology, 2-12-1-58-36 Ookayama, Meguro-ku, Tokyo 152-8552, Japan  
Email: hayakawa.t.ac@m.titech.ac.jp

† Electronic Supplementary Information (ESI) available: Synthetic procedure and characterization data of PGMA, PHETMA, PHFMA homopolymers, and PS-*r*-PMMA-*r*-PGMA random copolymer. DSC curves of PGMA, PHETMA, and PHFMA homopolymers. Determination of homopolymer densities by gradient column for PHETMA and PHFMA. Contact angle measurements and SFE estimations of PGMA, PHETMA, and PHFMA homopolymers. FT-IR spectra of SG19, SE22, and SF24. Temperature-dependent SAXS analyses of SG10, SE11, and SF6. Details of  $\chi_{\text{eff}}$  estimation. Etch contrast between PS and PHFMA. See DOI: 10.1039/x0xx00000x



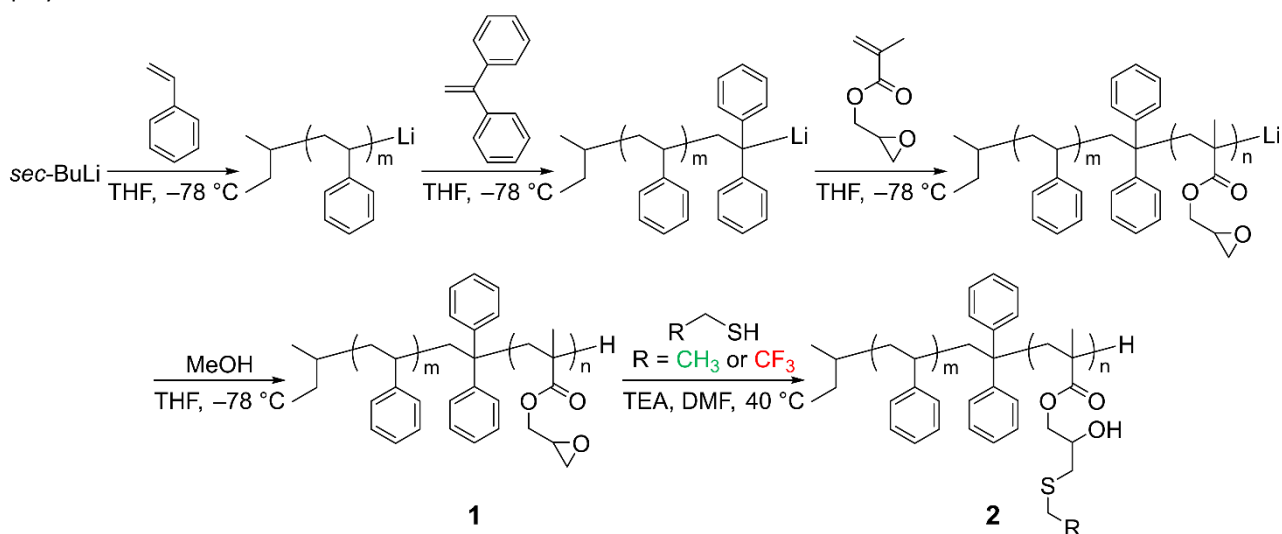
**Scheme 1** Concept for designing a chemically tailored high- $\chi$  BCP with balanced surface affinities and increased strengths of segregation.

the PGMA segment to obtain polystyrene-*block*-poly[2-hydroxy-3-(2,2,2-trifluoroethylsulfanyl)propyl methacrylate] (PS-*b*-PHFMA) (Scheme 2). PS-*b*-PHFMA consists of a moderately hydrophobic PS block and a PHFMA block that contains hydrophilic carboxylic ester, hydroxyl moieties, and a strongly hydrophobic fluorine-containing trifluoroethyl functionality. The PS domain should be incompatible with the hydrophilic and strongly hydrophobic moieties, while the trifluoroethyl-containing affinity control unit can be used to decrease the hydrophilicity of the PGMA segment. A small angle X-ray scattering (SAXS) analysis was used to determine  $\chi_{\text{eff}}$  via the random-phase approximation method, and the thin films of PS-*b*-PHFMA revealed the formation of well-ordered perpendicular lamellae as characterized by atomic force microscopy (AFM) and scanning electron microscopy (SEM).

## Experimental section

### Methods

The  $^1\text{H}$  and  $^{13}\text{C}$  nuclear magnetic resonance (NMR) spectra of the polymers were recorded on a JEOL 400 MHz NMR



**Scheme 2** Synthetic scheme of the PS-*b*-PGMA derivatives via the living anionic polymerization of styrene and glycidyl methacrylate and post-functionalization with thiols.

instrument using acetone- $d_6$  as a solvent. The number-average and weight-average molecular weights ( $M_n$  and  $M_w$ ) were measured by size exclusion chromatography (SEC) using a Shodex GPC-101 system equipped with a refractive index detector and a LF-804 column (Showa Denko) with tetrahydrofuran (THF) as the eluent. Fourier transform infrared spectra (FT-IR) were obtained with a JASCO FT/IR-4100 Fourier transform spectrophotometer. Differential scanning calorimetry (DSC) measurements were carried out using an EXSTAR7000 series DSC7020 (Hitachi High Tech) by heating the prepared samples at a rate of  $10\text{ }^\circ\text{C min}^{-1}$ . Thermogravimetric analyses (TGA) were conducted using an EXSTAR7000 series TG/DTA7300 (Hitachi High Tech) between 30 and  $500\text{ }^\circ\text{C}$  at a heating rate of  $10\text{ }^\circ\text{C min}^{-1}$ . Contact angle measurements were performed using a Kyowa DM-501YH, water, and diiodomethane. SAXS measurements were carried out using a Bruker NanoSTAR (50 kV/50 mA) with a 2D-PSPC detector (camera length of 1055 mm) to determine the morphology in the bulk and the temperature dependence of  $\chi_{\text{eff}}$ . Transmission electron microscopy (TEM) (H-7650, Hitachi High Tech) was used to examine the 60-nm thin slices produced by cryoultramicrotomy at  $-120\text{ }^\circ\text{C}$  (EM UC7 and EM FC7, Leica) and stained by ruthenium tetroxide ( $\text{RuO}_4$ ). The thin film samples were prepared using a MIKASA spin coater IH-D7, and the film thicknesses were measured by a FILMETRICS F20-EXR. AFM (NanoWizard Ultra Speed A, JPK) was used to observe the surface architectures of the BCP thin films. The tilted cross-section of the BCP thin film was observed using a field emission scanning electron microscope (FE-SEM) (S5500, Hitachi High Tech) after an oxygen reactive ion etching ( $\text{O}_2$ -RIE) treatment (Satoh Sinku).

### Materials

Lithium chloride (LiCl) was obtained from Kanto Chemical Co. Inc. and baked under a reduced pressure at  $200\text{ }^\circ\text{C}$  overnight before use. Styrene, 1,1-diphenylethylene (DPE), and glycidyl methacrylate (GMA) were purchased from Tokyo Chemical

Industry. Styrene and GMA were distilled over calcium hydride ( $\text{CaH}_2$ ). The purified styrene and GMA were further distilled over di-*n*-butyl magnesium and  $\text{CaH}_2$ , respectively. DPE was distilled over *n*-butyllithium. All other materials were reagent grade, purchased from Kanto Chemical Co. Inc., Tokyo Chemical Industry, FUJIFILM Wako Pure Chemical Corporation, and Sigma-Aldrich, and used as received. The detailed synthetic procedures of the homopolymers and the random copolymer are described in the ESI.

### Synthetic procedures

#### Synthesis of PS-*b*-PGMA by living anionic polymerization (1).

An example of the anionic polymerization of styrene and GMA is as follows. All polymerization procedures were performed under an argon purge. Here, 50 mL of THF and LiCl (28.7 mg, 0.678 mmol) were transferred to a 100-mL Schlenk flask and then cooled to  $-78^\circ\text{C}$ . *Sec*-butyllithium (*sec*-BuLi) was added until the color changed to light yellow. The Schlenk flask was removed from the cooling bath and allowed to reach room temperature, causing the solution to become colorless. The Schlenk flask was cooled to  $-78^\circ\text{C}$ , and *sec*-BuLi solution in cyclohexane and *n*-hexane (0.127 mL, 0.136 mmol) was added. Styrene (2.50 mL, 21.8 mmol) was added and stirred for 30 min, changing the solution color to bright orange. DPE (0.237 mL, 1.26 mmol) was added, resulting in a deep red color. After 30 min of stirring, GMA (1.08 mL, 8.18 mmol) was added and stirred for 30 min. The solution became colorless. Then, 5 mL of methanol (MeOH) (excess amount) purged with argon was added to the Schlenk flask to prepare the proton-terminated PS-*b*-PGMA. The polymer was precipitated into MeOH and filtered, and then the product was dried under a reduced pressure at  $40^\circ\text{C}$  overnight to yield PS-*b*-PGMA as a white powder (3.05 g, 89 % yield). The  $M_n$  and dispersity ( $\mathcal{D} = M_w/M_n$ ) of the product tested by SEC were  $19\,200\text{ g mol}^{-1}$  and 1.09, respectively.  $^1\text{H}$  NMR (400 MHz, acetone- $d_6$ ,  $\delta$ , ppm): 0.98 (s,  $\alpha\text{-CH}_3$ , PGMA), 1.14 (s,  $\alpha\text{-CH}_3$ , PGMA), 1.29–1.80 (br, backbone,  $-\text{CH}_2\text{-CH-}$ , PS), 1.84–2.30 (br, backbone,  $-\text{CH}_2\text{-CH-}$ , PS, br, backbone,  $-\text{CH}_2\text{-C}(\text{CH}_3)\text{-}$ , PGMA), 2.70 (s,  $-\text{CH}_2\text{-CH}(\text{CH}_2)\text{-O-}$ , PGMA), 2.82 (s,  $-\text{CH}_2\text{-CH}(\text{CH}_2)\text{-O-}$ , PGMA), 3.28 (s,  $-\text{CH}_2\text{-CH}(\text{CH}_2)\text{-O-}$ , PGMA), 3.84 (s,  $-(\text{C}=\text{O})\text{O-CH}_2\text{-}$ , PGMA), 4.37 (s,  $-(\text{C}=\text{O})\text{O-CH}_2\text{-}$ , PGMA), 6.39–6.85 (m, *o*-aromatic, PS) 6.91–7.42 (m, *m*-, *p*-aromatic, PS).  $^{13}\text{C}$  NMR (100 MHz, acetone- $d_6$ ,  $\delta$ , ppm): 17.8, 19.8, 41.7, 45.2, 46.0, 49.7, 55.0, 67.2, 127.0, 129.3, 146.4, 178.2. IR (KBr,  $\nu$ ,  $\text{cm}^{-1}$ ): 3026, 2925, 1731, 1602, 1493, 1453, 1255, 1237, 1172, 1150, 1132, 993, 907, 846, 758, 698, 540.

**Synthesis of polystyrene-*block*-poly(2-hydroxy-3-ethylsulfanylpropyl methacrylate) (PS-*b*-PHEtMA) and PS-*b*-PHFMA through the post-functionalization of PS-*b*-PGMA with ethanethiol or 2,2,2-trifluoroethanethiol (2).** The general procedure for the post-functionalization of PS-*b*-PGMA is as follows. A 10-mL round bottom flask was charged with PS-*b*-PGMA and *N,N*-dimethylformamide (DMF) (20 mole equiv. to PGMA repeating units) and immersed in an ice-water bath. Triethylamine (TEA) (2 mole equiv.) and ethanethiol or 2,2,2-trifluoroethanethiol (2 mole equiv.) were added to the flask. After 30 min, the flask was transferred to an oil bath set to  $40^\circ\text{C}$  and stirred for 24 h. The crude solution was diluted with THF,

precipitated from an MeOH/water mixture, and then filtered to collect the precipitate. After filtration, the solid was dissolved in THF, precipitated from an MeOH/water mixture, and then filtered 2 or 3 times to remove the residual reagents. The product was dried under a reduced pressure at room temperature overnight to yield a white powder (70% yield).

**Characterization of PS-*b*-PHEtMA.**  $^1\text{H}$  NMR (400 MHz, acetone- $d_6$ ,  $\delta$ , ppm): 0.99 (s,  $\alpha\text{-CH}_3$ , PHEtMA), 1.13 (s,  $\alpha\text{-CH}_3$ , PHEtMA), 1.29 (t,  $-\text{S-CH}_2\text{-CH}_3$ ), 1.37–1.75 (br, backbone,  $-\text{CH}_2\text{-CH-}$ , PS), 1.82–2.29 (br, backbone,  $-\text{CH}_2\text{-CH-}$ , PS, br, backbone,  $-\text{CH}_2\text{-C}(\text{CH}_3)\text{-}$ , PHEtMA), 2.56–2.71 (q,  $-\text{S-CH}_2\text{-CH}_3$ , PHEtMA), 2.72–2.90 (m,  $-\text{CH}(\text{OH})\text{-CH}_2\text{-S-}$ , PHEtMA), 3.89–4.22 (m,  $-(\text{C}=\text{O})\text{O-CH}_2\text{-CH}(\text{OH})\text{-}$ , PHEtMA), 4.38 (s,  $-\text{OH}$ , PHEtMA), 6.41–6.83 (m, *o*-aromatic, PS), 6.91–7.34 (m, *m*-, *p*-aromatic, PS).  $^{13}\text{C}$  NMR (100 MHz, acetone- $d_6$ ,  $\delta$ , ppm): 15.6, 17.9, 27.3, 36.1, 41.5, 45.8, 54.6, 68.6, 69.6, 126.7, 129.0, 146.0, 177.6, 178.2. IR (KBr,  $\nu$ ,  $\text{cm}^{-1}$ ): 3438, 3026, 2924, 1728, 1602, 1493, 1452, 1269, 1154, 1072, 754, 698, 540.

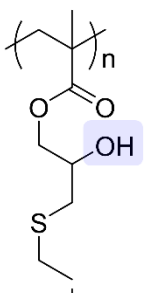
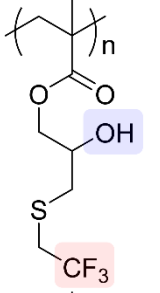
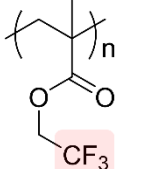
**Characterization of PS-*b*-PHFMA.**  $^1\text{H}$  NMR (400 MHz, acetone- $d_6$ ,  $\delta$ , ppm): 0.98 (s,  $\alpha\text{-CH}_3$ , PHFMA), 1.12 (s,  $\alpha\text{-CH}_3$ , PHFMA), 1.26–1.74 (br, backbone,  $-\text{CH}_2\text{-CH-}$ , PS), 1.82–2.30 (br, backbone,  $-\text{CH}_2\text{-CH-}$ , PS, br, backbone,  $-\text{CH}_2\text{-C}(\text{CH}_3)\text{-}$ , PHFMA), 2.86–3.02 (m,  $-\text{CH}(\text{OH})\text{-CH}_2\text{-S-}$ , PHFMA), 3.40–3.59 (q,  $-\text{S-CH}_2\text{-CF}_3$ , PHFMA), 3.85–4.20 (m,  $-(\text{C}=\text{O})\text{O-CH}_2\text{-CH}(\text{OH})\text{-}$ , PHFMA), 4.60 (s,  $-\text{OH}$ , PHFMA), 6.39–6.82 (m, *o*-aromatic, PS), 6.92–7.32 (m, *m*-, *p*-aromatic, PS).  $^{13}\text{C}$  NMR (100 MHz, acetone- $d_6$ ,  $\delta$ , ppm): 18.0, 19.8, 34.5, 34.9, 35.2, 35.5, 37.2, 41.6, 45.8, 46.1, 54.6, 68.5, 69.9, 123.5, 126.3, 126.7, 128.6, 129.0, 131.7, 146.1, 178.1. IR (KBr,  $\nu$ ,  $\text{cm}^{-1}$ ): 3470, 3026, 2925, 1730, 1602, 1494, 1453, 1409, 1315, 1271, 1246, 1125, 1082, 1028, 995, 842, 755, 697, 637, 536.

### Bulk film preparation

The Bulk films used to investigate the bulk morphologies and domain spacings (*d*-spacing) of the microphase-separated structures were prepared by slowly evaporating a dilute BCP solution dissolved in THF at  $40^\circ\text{C}$  and drying under a reduced pressure before annealing at  $150^\circ\text{C}$  for 24 h.

### Thin film preparation

Silicon wafers were cut into  $1\text{-cm}^2$  pieces, sonicated in toluene for 3 min, and dried in a stream of nitrogen. The substrates were treated with a mixture of  $\text{H}_2\text{O}_2$  (30 %) and  $\text{H}_2\text{SO}_4$  (70 %) (v/v) at  $80^\circ\text{C}$  for 30 min. The wafers were rinsed with water, ethanol, and water again and dried in a stream of nitrogen. Random copolymer layers were generated by spin-coating a 1.0 wt.% polystyrene-*random*-poly(methyl methacrylate)-*random*-poly(glycidyl methacrylate) (PS-*r*-PMMA-*r*-PGMA) solution in toluene at 3000 rpm and 30 s onto the cleaned silicon wafers, followed by crosslinking at  $160^\circ\text{C}$  for 24 h. The substrates were sonicated in toluene to remove the random copolymers that were not attached and rinsed with fresh toluene. Here, 1.2 wt.% solutions of the BCPs (SE22 and SF24) in toluene were spin-coated at 3000 rpm for 30 s onto the surface-modified silicon substrates to obtain thin films with ca.  $1 L_0$  thicknesses (one period of the lamellar domain). The thin films were annealed at  $120^\circ\text{C}$  for 10 min under ambient conditions. An  $\text{O}_2$ -RIE

Chemical Structures of the Homopolymers	SFEs ( $\text{mJ m}^{-2}$ )
 <p>PHEtMA</p>	44.2 <sup>a</sup>
 <p>PHFMA</p>	33.3 <sup>a</sup>
 <p>PTFEMA</p>	25.1 <sup>b</sup>

**Scheme 3** Chemical structures and surface free energies of the homopolymers: <sup>a</sup> estimated by the contact angle measurements and the Owens–Wendt method and <sup>b</sup> the reported value in ref. 44.

treatment was conducted for 50 s (20 sccm, 20 W, 20 Pa) to selectively remove the methacrylate block (The details regarding the etch contrast are described in the ESI.). The cross-sections of the etched thin films were prepared by freeze-fracturing in liquid nitrogen.

## Results and discussion

### Synthesis and characterization of the homopolymers

Prior to the synthesis of the BCPs, the homopolymers were synthesized, and the surface properties were characterized. The parent precursor homopolymers PGMA were prepared by the anionic polymerization of GMA using *sec*-BuLi as an initiator in the presence of excess amounts of LiCl and DPE at  $-40\text{ }^{\circ}\text{C}$  in THF under argon.<sup>36,37</sup> Subsequently, homopolymers of PHFMA and poly(2-hydroxy-3-ethylsulfanylpropyl methacrylate) (PHEtMA), fluorinated and non-fluorinated analogues of each other, were synthesized by the post-polymerization thiol-epoxy click reaction of PGMA with 2,2,2-trifluoroethanethiol or ethanethiol in DMF with TEA as a catalyst at  $40\text{ }^{\circ}\text{C}$  for 24 h.<sup>38–42</sup> The ring-opening nature of the functionalization of PGMA introduces hydrophilic hydroxyl moieties, in addition to the functionalities on the thiol reagent, onto each repeating unit. The synthesized homopolymers were then characterized by NMR, SEC, DSC, and

TGA. The glass transition temperatures ( $T_g$ ) of the homopolymers, as determined from the base-line shifts in the DSC measurements, were 68, 25, and  $37\text{ }^{\circ}\text{C}$  for PGMA, PHEtMA, and PHFMA, respectively (Fig. S2), whereas the 5 wt.% decomposition temperatures for PGMA, PHEtMA, and PHFMA were recorded in the TGA analyses as 320, 303, and  $316\text{ }^{\circ}\text{C}$ , respectively. Furthermore, the densities of PHEtMA and PHFMA were  $1.23$  and  $1.43\text{ g cm}^{-3}$ , respectively, using homopolymers in the density gradient columns prepared from aqueous potassium iodide solution and calibrated with the densities of known organic reagents at room temperature (The details are available in the ESI.).

The surface free energies (SFEs) of PGMA, PHEtMA, and PHFMA, estimated via the water and diiodomethane contact angle measurements based on the Owens–Wendt method,<sup>43</sup> were  $51.1$ ,  $44.2$ , and  $33.3\text{ mJ m}^{-2}$  for PGMA, PHEtMA, and PHFMA, respectively. For a comparison, the chemical structure of poly(2,2,2-trifluoroethyl methacrylate) (PTFEMA), which is

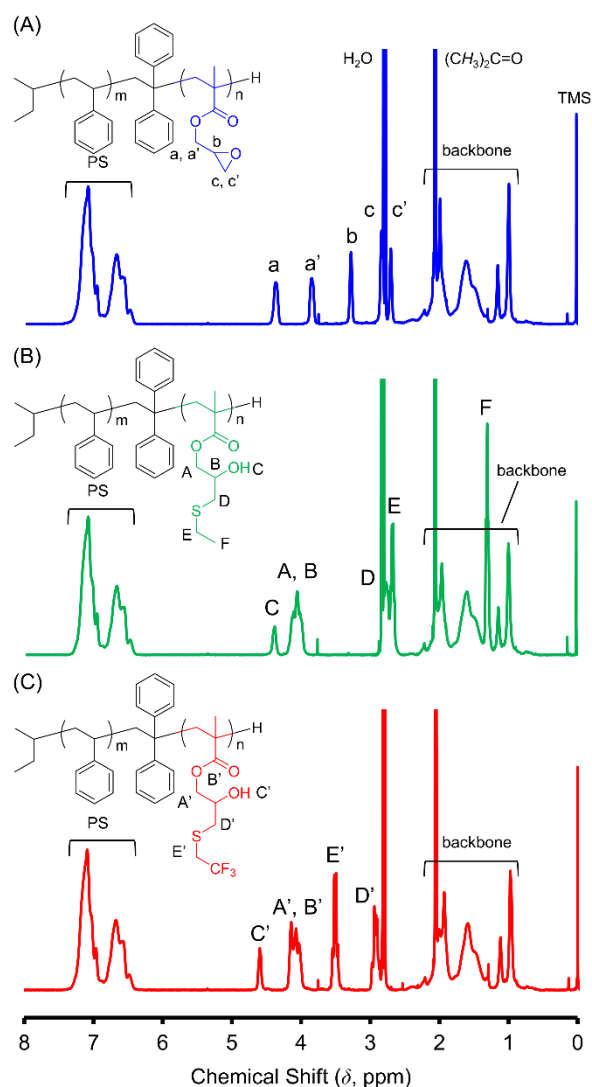


**Fig. 1**  $^1\text{H}$  NMR spectra of (A) PS-*b*-PGMA (SG19), (B) PS-*b*-PHEtMA (SE22), and (C) PS-*b*-PHFMA (SF24).

comprised of methacrylate repeating units functionalized with trifluoroethyl moieties, is similar to PHFMA without hydroxyl functionalities. The SFE for PTFEMA, measured using the same method, was  $25.1 \text{ mJ m}^{-2}$ .<sup>44</sup> This suggested that the introduction of the hydrophobic trifluoroethyl functionality significantly decreased the SFE of the hydrophilic polymer from  $51.1 \text{ mJ m}^{-2}$  in the parent precursor polymer, PGMA, to  $33.3 \text{ mJ m}^{-2}$  in PHFMA. However, because of the hydrophilic hydroxyl and hydrophobic trifluoroethyl moieties on each repeating unit, the SFE of PHFMA is the averaged SFE of the analogous polymers containing only the hydroxyl (PHetMA) or the trifluoroethyl (PTFEMA) functionalities (Scheme 3). These results suggest that the hydrophobic trifluoroethyl affinity control unit managed to counteract the relative hydrophilicity of the hydroxyl functionality, balancing the SFE of the PHFMA block.

### Synthesis and characterization of the BCPs

A series of PS-*b*-PGMA parent precursor polymers (SG19–SG2) was successfully synthesized by the sequential anionic polymerization of styrene and GMA using *sec*-BuLi in excess amounts of LiCl and DPE at  $-78 \text{ }^\circ\text{C}$  in THF under argon (Scheme 2)<sup>36,37</sup> and PS-*b*-PGMAs were characterized by NMR (Fig. 1A). The  $M_n$  and  $\mathcal{D}$  of the PS-*b*-PGMAs were obtained by SEC using THF as the eluent based on PS standards. The PS volume fractions ( $f_{\text{PS}}$ ) were calculated via  $^1\text{H}$  NMR (Table 1), based on the densities of  $1.05 \text{ g cm}^{-3}$  and  $0.805 \text{ g cm}^{-3}$  for PS and PGMA, respectively.<sup>45</sup> The synthesized BCPs exhibited molecular weights ranging from  $20 \text{ kg mol}^{-1}$  to  $2 \text{ kg mol}^{-1}$  with narrow dispersities.

The PS-*b*-PGMA parent precursor polymers were then functionalized via a ring-opening reaction with 2,2,2-trifluoroethanethiol in DMF with TEA as a catalyst at  $40 \text{ }^\circ\text{C}$  for 24 h to yield PS-*b*-PHFMAs (Scheme 2).<sup>38–42</sup> As a control, the

non-fluorinated analogue was also synthesized to yield PS-*b*-PHetMA. Compared to the parent precursor polymer, the  $M_n$  of the functionalized BCPs increased after the introduction of the affinity control units, while the dispersities remained constant (Table 1). According to the  $^1\text{H}$  NMR analysis (Fig. 1), signals a, a', b, c, and c' attributed to the glycidyl group (2.70, 2.82, 3.28, 3.84, and 4.37 ppm, respectively) for PS-*b*-PGMA (Fig. 1A) were completely disappeared in the spectra for PS-*b*-PHetMA and PS-*b*-PHFMA (Fig. 1B and C, respectively). In addition, new signals A–F, corresponding to the protons of PHetMA (A and B: 3.89–4.22 ppm, C: 4.38 ppm, D and E: 2.56–2.90 ppm, and F: 1.29 ppm in Fig. 1B), and A'–E', corresponding to the protons of PHFMA (A' and B': 3.85–4.22 ppm, C': 4.60 ppm, D': 2.86–3.02 ppm, and E': 3.40–3.59 ppm in Fig. 1C), appeared, suggesting that the post-functionalization of PGMA proceeded successfully. The complete ring-opening of the glycidyl group was also supported by FT-IR characterization (Fig. S4). Peaks appearing at  $907$  and  $846 \text{ cm}^{-1}$  in the FT-IR spectrum of PS-*b*-PGMA, which corresponded to C–O–C stretching in oxirane, disappeared in the FT-IR spectra of the functionalized BCPs. In addition, a broad peak in the  $3500 \text{ cm}^{-1}$  region, corresponding to O–H stretching, appeared in the spectra of the functionalized BCPs. Furthermore, peaks ascribed to C–F stretching were observed at  $1315$ ,  $1125$ ,  $1082$ ,  $842$ , and  $637 \text{ cm}^{-1}$  in the spectrum for PS-*b*-PHFMA. The  $f_{\text{PS}}$  of the PS-*b*-PGMA derivatives were calculated via the  $^1\text{H}$  NMR spectra based on the densities of  $1.05 \text{ g cm}^{-3}$  for PS,  $1.23 \text{ g cm}^{-3}$  for PHetMA, and  $1.43 \text{ g cm}^{-3}$  for PHFMA.

According to the NMR, SEC, and FT-IR analyses, PS-*b*-PGMAs, PS-*b*-PHetMAs, and PS-*b*-PHFMAs with well-defined primary structures were successfully prepared by combining living anionic polymerization with thiol-epoxy click reactions.

**Table 1** Characterization data of the synthesized BCPs.

BCP	Label <sup>a</sup>	$M_n^b$ (kg mol <sup>-1</sup> )	$\mathcal{D}^b$	$f_{\text{PS}}^c$	$d$ -spacing <sup>d</sup> (nm)	Morphology <sup>e</sup>
PS- <i>b</i> -PGMA	SG19	19.2	1.09	0.60	22.4	Lamella
	SG14	13.8	1.10	0.60	16.7	Lamella
	SG10	9.8	1.15	0.61	13.3	Lamella
	SG4	4.4	1.26	0.65	–	Disorder
	SG2	2.2	1.35	0.61	–	Disorder
PS- <i>b</i> -PHetMA	SE22	22.0	1.14	0.62	22.9	Lamella
	SE15	15.0	1.14	0.65	18.2	Lamella
	SE11	11.0	1.19	0.64	14.2	Lamella
	SE5	5.4	1.25	0.66	–	Disorder
	SE3	2.7	1.35	0.62	–	Disorder
PS- <i>b</i> -PHFMA	SF24	23.8	1.14	0.57	26.0	Lamella
	SF17	17.2	1.12	0.58	20.3	Lamella
	SF13	12.9	1.13	0.57	16.1	Lamella
	SF6	6.0	1.18	0.62	9.6	Lamella
	SF4	3.7	1.21	0.52	–	Disorder

<sup>a</sup> The labels SG, SE, and SF refer to PS-*b*-PGMA, PS-*b*-PHetMA, and PS-*b*-PHFMA, respectively, while the number to the right refers to the number-average molecular weight ( $M_n$ ) of the polymer. <sup>b</sup> The  $M_n$  and dispersities ( $\mathcal{D}$ ) were obtained by SEC using THF as the eluent based on PS standards. <sup>c</sup> The PS volume fractions ( $f_{\text{PS}}$ ) were calculated via  $^1\text{H}$  NMR based on the densities of  $1.05 \text{ g cm}^{-3}$  for PS,  $0.805 \text{ g cm}^{-3}$  for PGMA,  $1.23 \text{ g cm}^{-3}$  for PHetMA, and  $1.43 \text{ g cm}^{-3}$  for PHFMA. <sup>d</sup> The lamellar domain spacings ( $d$ -spacing) were estimated from the first-order peak position in the SAXS profile. <sup>e</sup> The morphologies in the bulk were determined by SAXS.

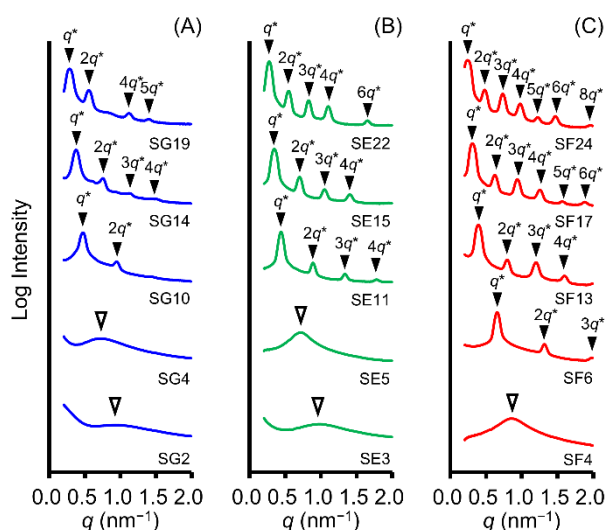


**Fig. 2** SAXS profiles of the (A) PS-*b*-PGMA, (B) PS-*b*-PHEtMA, and (C) PS-*b*-PHFMA bulk samples.

### Morphologies in the bulk

The morphologies of the microphase-separated structures formed in the bulk films of the synthesized BCPs were analyzed via SAXS and TEM. The bulk films were prepared from the slow

evaporation of dilute BCP solutions in THF and characterized after thermal annealing under a reduced pressure at 150 °C for 24 h, well above the  $T_g$  of all components (PS: 100 °C,<sup>46</sup> PGMA: 68 °C, PHEtMA: 25 °C, and PHFMA: 37 °C). The 2-D SAXS profiles taken at room temperature were azimuthally integrated to provide 1-D scattering profiles (Fig. 2) and analyzed using the Bragg equation ( $q = 4\pi\sin(\vartheta/2)/\lambda$ ), where  $\vartheta$  is the scattering angle, and  $\lambda$  is the wavelength. The domain-spacings ( $d$ -spacing, Table 1) for each BCP were calculated based on the position of the first-order scattering peak ( $q^*$ ) ( $d$ -spacing =  $2\pi/q^*$ ). The SAXS profiles of the higher molecular weight BCPs ( $M_n > 10$  kg mol<sup>-1</sup>) and SF6 exhibited sharp peaks, which were labelled with upside-down black triangles at the integer ratios to the first-order peaks, suggesting the formation of well-ordered lamellar structures. The first-order scattering peaks for the functionalized PS-*b*-PHEtMA and PS-*b*-PHFMA shifted leftwards compared to that of the PS-*b*-PGMA parent precursor polymers, corresponding to an increase in the  $d$ -spacing of the nanostructures. The  $d$ -spacing is scaled by  $\chi_{\text{eff}}^{1/6}N^\alpha$ , where  $N$  is the degree of polymerization normalized over the volume, and  $\alpha = 2/3$  or  $1/2$  in the strong or weak segregation regimes.<sup>47</sup> Therefore, the increase in the  $d$ -spacing of the functionalized BCPs suggested that  $\chi_{\text{eff}}N$  increased after the functionalization process. In contrast, the SAXS profiles for the lower molecular weight BCPs ( $M_n < 10$  kg mol<sup>-1</sup>), except that of SF6, exhibited a single, broad first-order peak, suggesting that disordered

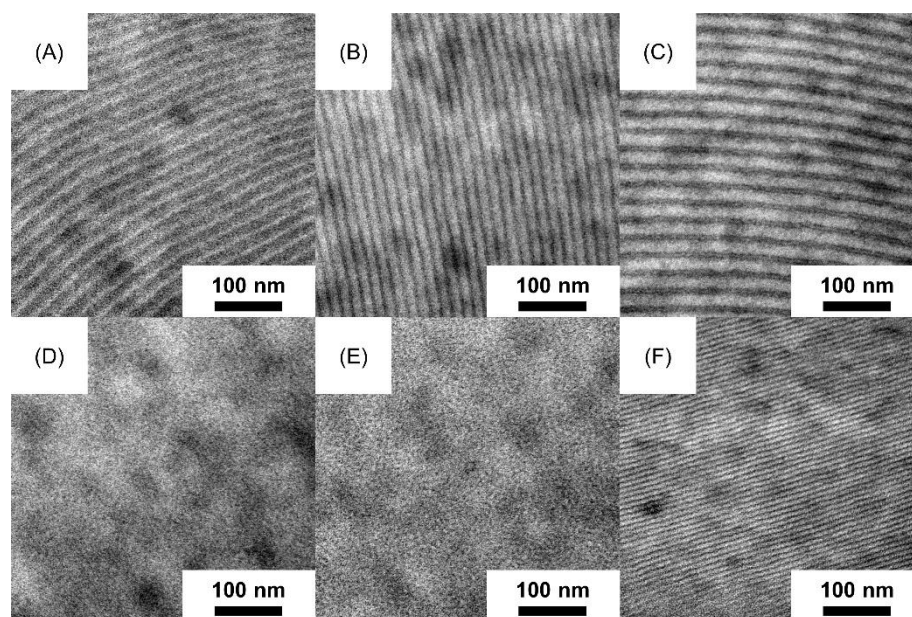


**Fig. 3** TEM images of PS-*b*-PGMA (A: SG19 and D: SG4), PS-*b*-PHEtMA (B: SE22 and E: SE5), and PS-*b*-PHFMA (C: SF24 and F: SF6). The dark regions correspond to the PS block owing to RuO<sub>4</sub> staining.

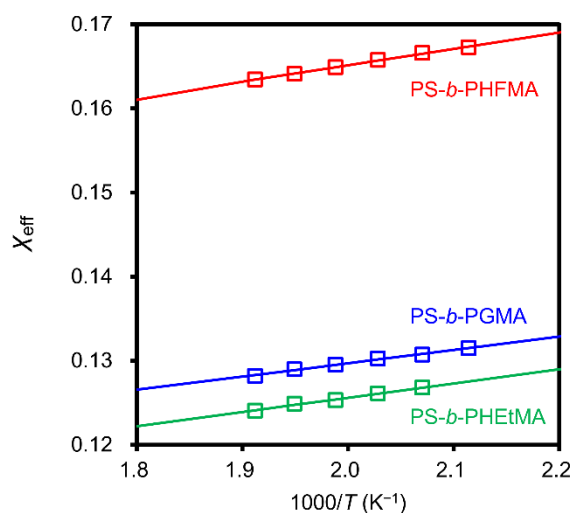


**Fig. 4** Temperature dependences of the effective Flory–Huggins interaction parameter for SG4 (blue line), SE5 (green line), and SF4 (red line) using a reference volume of  $118 \text{ \AA}^3$ .

structures had formed. Sample SF6 exhibited sharp scattering peaks ascribed to lamellae, as observed in the profiles of the higher molecular weight samples. Furthermore, the  $d$ -spacing was 9.6 nm, suggesting that well-ordered lamellae with sub-5-nm features had formed. Thin sections of the bulk films, prepared by cryoultramicrotomy, were also characterized using TEM after  $\text{RuO}_4$  staining. Linear structures were observed in the images of the higher molecular weight samples, SG19 (Fig. 3A), SE22 (Fig. 3B), and SF24 (Fig. 3C), suggesting that well-ordered lamellar structures had formed. Meanwhile, disordered morphologies were observed for the lower molecular weight SG4 (Fig. 3D) and SE5 (Fig. 3E) samples. However, highly-ordered lamellar structures with ca. 10 nm periodicities were observed for the fluorinated SF6 (Fig. 3F) sample, despite sharing the same parent precursor polymer as SE5, SG4. The TEM analyses agreed well with the SAXS results.

These morphological studies in the bulk suggest that the fluorination of PGMA strengthened the repulsion between the segments of the chemically tailored BCP, as single nanometer features could form despite the low molecular weight ( $M_n = 6 \text{ kg mol}^{-1}$ ) of the BCP. This suggested that the design concept (Scheme 1) is a promising tool for effectively developing BCPs that could resolve an important criterion for next-generation lithographic technologies.

#### Estimation of $\chi_{\text{eff}}$

The strength of the segregation of PGMA, PHEtMA, and PHfMA against PS was quantified by the random-phase approximation method in terms of the effective Flory–Huggins interaction parameter, expressed by  $\chi_{\text{eff}} = A/T + B$ , where  $A/T$  is the enthalpic contribution, and  $B$  is the entropic contribution.<sup>48–50</sup> Using this method, SAXS measurements need to be carried out at temperatures higher than the mean-field crossover

temperature to avoid thermal fluctuation effects. Firstly, temperature-dependent SAXS analyses were conducted on SG10, SE11, and SF6 starting from 250 °C and in 10 °C decrements (Fig. S5). The intensity of the first-order scattering peak was found to be lower only at around 240–250 °C for SG10, whereas a second-order scattering peak with a  $q:q^*$  ratio of 1:2 remained at 250 °C for SE11. Therefore, the order-disorder transition (ODT) could not be observed in SG10 and SE11, likely owing to the relatively higher molecular weights of the BCPs. However, the SAXS profiles of SF6 showed a discontinuous change in the  $I_{\text{max}}^{-1}-T^{-1}$  plot at 220 °C, as typically observed in BCP ODTs (Fig. S5D and E). Additionally, since these samples did not show mean-field disordered behavior at this temperature range,  $\chi_{\text{eff}}$  was estimated using the slightly lower molecular weight SG4, SE5, and SF4 samples. Discontinuous changes attributed to the transition from mean-field to non-mean-field type disordered states were observed at 190–200 °C for SG4 and SF4, and 200–210 °C for SE5 in the  $I_{\text{max}}^{-1}-T^{-1}$  plots for each sample (Fig. S6). The SAXS profiles in the mean-field disordered state were then analyzed based on Leibler’s mean-field theory modified to include the effects from the molecular weight dispersity and asymmetry in the segmental volume.<sup>48–50</sup> Here, because  $\chi_{\text{eff}}$  is dependent on the reference volume used to calculate  $N$ , a common reference volume ( $v_0 = 118 \text{ \AA}^3$ ) was utilized to compare the  $\chi_{\text{eff}}$  values with other reported values. A linear least-squares fit of the data for SG4, SE5, and SF4 (Fig. S7) yielded the temperature dependences of  $\chi_{\text{eff}}$  (Fig. 4), and each term is listed in Table S5. The estimated  $\chi_{\text{eff}}$  values for SG4 and SE5 showed similar values of 0.151 and 0.149, respectively, at 25 °C. In contrast,  $\chi_{\text{eff}}$  for SF4, as expressed by  $\chi_{\text{eff SF4}} = 19.4/T + 0.126$  was larger than those of the non-fluorinated samples (0.191 at 25 °C). Based on these results,  $\chi_{\text{eff}}N$  for SG4, SE5, and SF6 were 9.6, 10.2, and 13.6, respectively. Since BCP self-assembly is expected to occur at  $\chi_{\text{eff}}N$  above 10.5, these results quantitatively explain why only the lower molecular weight SF6 sample ( $\chi_{\text{eff}}N = 13.6$ ) was capable of self-assembling into sub-5-nm structures. Compared to the reported  $\chi_{\text{eff}}$  value of 0.04 for PS-*b*-PMMA at 25 °C,<sup>33</sup> PS-*b*-PHfMA, which consists of the same PS and methacrylate backbone with additional hydroxyl and trifluoroethyl functionalities, exhibited an  $\chi_{\text{eff}}$  value 4.8 times greater than that of PS-*b*-PMMA. Although the hydroxyl and trifluoroethyl moieties cancelled each other out to balance the SFE of PHfMA, the strength of segregation and chemical incompatibility against PS increased owing to the addition of the chemically disparate hydroxyl and trifluoroethyl functionalities.

#### Nanostructures and domain orientation in thin films

To investigate the effects of fluorination on the self-assembly behavior in the thin films, the SE22 and SF24 thin films were prepared. First, the BCPs were spin-coated onto bare silicon wafers from 1.2 wt.% toluene solutions and annealed at 120 °C for 10 min under ambient conditions. In the AFM images (Fig. 5) for the SE22 thin film, a flat featureless surface was observed, whereas hole structures with a 1.0 and 0.5 period of lamellar domain ( $L_0$ ) height differences and opposite phases were observed on the SF24 thin film. These data suggested that parallel structures had formed in both thin films. However, the



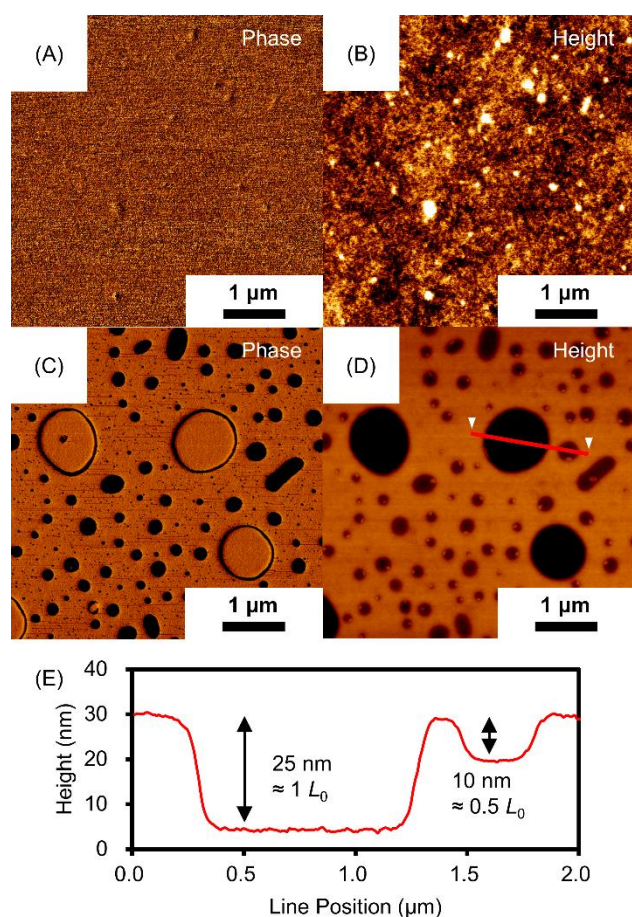


**Fig. 5** AFM phase and height images for the (A and B) SE22 and (C and D) SF24 thin films prepared on bare Si after thermal annealing at 120 °C for 10 min. Image (E) shows the cross-sectional profile of the red line in D.

appearance of holes with the 1.0 and 0.5  $L_0$  height differences and opposing phases in the SF24 thin film suggested that the air interface is near-neutral for both segments, while the substrate is preferential towards one segment.<sup>51</sup> Hence, PS-*r*-PMMA-*r*-PGMA (PS:PMMA:PGMA = 51:48:1 mole fraction) were spin-coated onto bare silicon wafers and crosslinked to neutralize any preferential affinity of the substrate.<sup>52,53</sup> The BCPs were then spin-coated from 1.2 wt.% toluene solutions and annealed at 120 °C for 10 min under ambient conditions. The AFM image (Fig. 6A) for the SE22 thin film showed a rough featureless surface owing to the selective segregation of one segment onto the free surface. Conversely, a fingerprint pattern was observed on the SF24 thin film, suggesting that perpendicular lamellae had formed (Fig. 6B). Compared to the SFE of PS, reported to be 40.7 mJ m<sup>-2</sup> at 25 °C,<sup>54</sup> the measured SFE of PHFMA, at 33.3 mJ m<sup>-2</sup>, is relatively different. Nevertheless, the formation of perpendicular lamellae could be attributed to the temperature dependence of the SFE. It is speculated that, at high temperatures (120 °C), the difference in the SFE between PS and PHFMA is significantly decreased, such that the surface affinities of both PS and PHFMA are close enough to satisfy the neutrality condition required for perpendicular orientation. To obtain

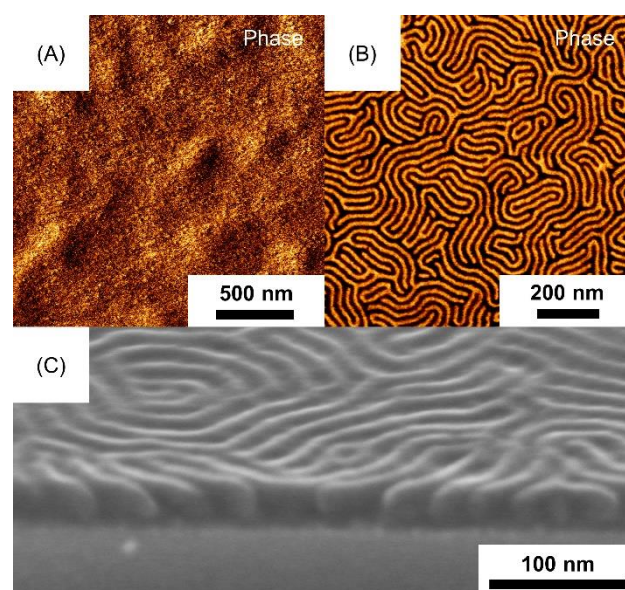


**Fig. 6** AFM phase images of the (A) SE22 and (B) SF24 thin films prepared on chemically-modified Si wafers after thermal annealing at 120 °C for 10 min. Image (C) shows the tilted-SEM image of the SF24 thin film after O<sub>2</sub>-RIE treatment.

further information regarding the internal structure of the SF24 thin film, an O<sub>2</sub>-RIE treatment was conducted to selectively remove the PHFMA domain, and the thin film was characterized using SEM (The etch contrast between PS and PHFMA is described in the ESI.). In the SEM image of the tilted thin film (Fig. 6C), a fingerprint pattern with the PHFMA domain removed was observed, implying that the perpendicular lamellae had stretched from the surface to the substrate. With further optimization of the thin film processing conditions for the lowest molecular weight BCPs, we can expect to prepare sub-5-nm half-pitch patterns for future lithographic applications.

## Conclusions

In this study, a design concept to chemically tailor the surface affinities and strength of segregation of a BCP system was proposed to enable perpendicular lamellae on thin films using thermal annealing processes for BCP lithography applications. Because of the ease of post-functionalization and strongly segregating hydrophobic-hydrophilic blocks, a parent precursor polymer, PS-*b*-PGMA, was synthesized via the sequential living anionic polymerization of styrene and glycidyl methacrylate. The glycidyl moieties on the PGMA block were then functionalized with 2,2,2-trifluoroethanethiol to obtain PS-*b*-PHFMA, which contains hydrophilic hydroxyl groups and hydrophobic trifluoroethyl functionalities. The SAXS and TEM analyses of the bulk PS-*b*-PHFMA films revealed well-ordered lamellae with a minimum  $d$ -spacing of 9.6 nm. Based on the random-phase approximation and using a reference volume of 118 Å<sup>3</sup> to normalize the degree of polymerization over the volume, the temperature dependence of the effective Flory-Huggins interaction parameter was estimated to be  $\chi_{\text{eff}}^{\text{S/PHFMA}} =$

19.4/T + 0.126, and  $\chi_{\text{eff}}$  was 0.191 at 25 °C. From the thin film studies, the formation of perpendicular lamellae on surface-modified silicon wafers was demonstrated using only thermal annealing at 120 °C for 10 min. These results show that by chemically tailoring the hydrophilic PGMA block of PS-*b*-PGMA with the introduction of hydrophobic trifluoroethyl functionalities, the surface affinity of the PHFMA block relative to the hydrophobic PS was neutralized, facilitating the formation of perpendicular structures on thin films via thermal annealing. The carboxylic ester, hydroxyl, and trifluoroethyl functionalities also increased the chemical incompatibility of PHFMA against PS, increasing the strength of segregation. Based on a design concept, a chemically tailored high- $\chi$  BCP, PS-*b*-PHFMA, capable of orienting perpendicularly on thin films through facile thermal annealing under ambient conditions was prepared. By chemically tailoring the BCP to fulfill the sub-5-nm resolution and perpendicular orientation requirements, PS-*b*-PHFMA has proven to be a strong candidate for next-generation BCP lithography resists.

### Conflicts of interest

There are no conflicts to declare.

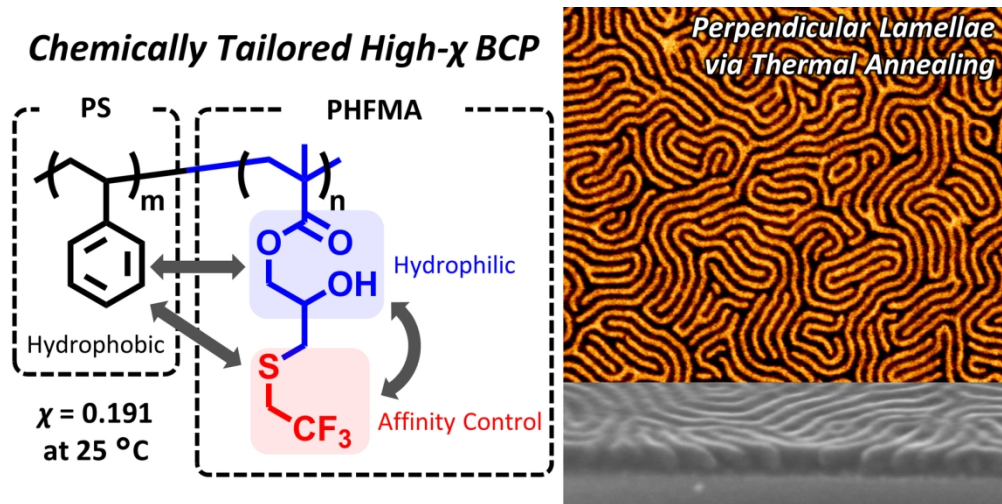
### Acknowledgements

This research was supported in part by the Japan Science and Technology Agency (JST), Precursory Research for Embryonic Science and Technology (PRESTO) on the Molecular Technology and Creation of New Functions, Grant-in-Aid for Scientific Research (B) (JSPS KAKENHI Grant Number 17H03113), JSPS KAKENHI for Scientific research on Innovative Areas "Materials Science on Mille-feuille Structure (MFS)" (Grant Number JP18H05482), and the Ogasawara Foundation for the Promotion of Science & Engineering. The atomic force microscopy experiments were supported by the New Energy and Industrial Technology Development Organization (NEDO) in Japan under the EIDEC project. The authors would like to thank Prof. Yuji Wada of the Tokyo Institute of Technology and Ryohei Kikuchi and Jun Koki of the Tokyo Institute of Technology Ookayama Materials Analysis Division for support with the SEM and TEM measurements.

### References

- H. C. Kim, S. M. Park and W. D. Hinsberg, *Chem. Rev.*, 2010, **110**, 146–177.
- C. M. Bates, M. J. Maher, D. W. Janes, C. J. Ellison and C. G. Willson, *Macromolecules*, 2014, **47**, 2–12.
- G. Jeong, D. M. Yu, J. K. D. Mapas, Z. Sun, J. Rzayev and T. P. Russell, *Macromolecules*, 2017, **50**, 7148–7154.
- J. K. D. Mapas, T. Thomay, A. N. Cartwright, J. Ilavsky and J. Rzayev, *Macromolecules*, 2016, **49**, 3733–3738.
- J. G. Kennemur, L. Yao, F. S. Bates and M. A. Hillmyer, *Macromolecules*, 2014, **47**, 1411–1418.
- D. P. Sweat, M. Kim, S. R. Larson, J. W. Choi, Y. Choo, C. O. Osuji and P. Gopalan, *Macromolecules*, 2014, **47**, 6687–6696.
- Y. Luo, D. Montarnal, S. Kim, W. Shi, K. P. Barteau, C. W. Pester, P. D. Hustad, M. D. Christianson, G. H. Fredrickson, E. J. Kramer and C. J. Hawker, *Macromolecules*, 2015, **48**, 3422–3430.
- M. C. D. Carter, J. Jennings, F. W. Speetjens, D. M. Lynn and M. K. Mahanthappa, *Macromolecules*, 2016, **49**, 6268–6276.
- A. P. Lane, X. Yang, M. J. Maher, G. Blachut, Y. Asano, Y. Someya, A. Mallavarapu, S. M. Sirard, C. J. Ellison and C. G. Willson, *ACS Nano*, 2017, **11**, 7656–7665.
- J. Kwak, A. K. Mishra, J. Lee, K. S. Lee, C. Choi, S. Maiti, M. Kim and J. K. Kim, *Macromolecules*, 2017, **50**, 6813–6818.
- S. Jo, S. Jeon, T. Jun, C. Park and D. Y. Ryu, *Macromolecules*, 2018, **51**, 7152–7159.
- K. Azuma, J. Sun, Y. Choo, Y. Rokhlenko, J. H. Dwyer, B. Schweitzer, T. Hayakawa, C. O. Osuji and P. Gopalan, *Macromolecules*, 2018, **51**, 6460–6467.
- J. D. Cushen, I. Otsuka, C. M. Bates, S. Halila, S. Fort, C. Rochas, J. A. Easley, E. L. Rausch, A. Thio, R. Borsali, C. G. Willson and C. J. Ellison, *ACS Nano*, 2012, **6**, 3424–3433.
- J. G. Kennemur, M. A. Hillmyer and F. S. Bates, *Macromolecules*, 2012, **45**, 7228–7236.
- J. D. Cushen, C. M. Bates, E. L. Rausch, L. M. Dean, S. X. Zhou, C. G. Willson and C. J. Ellison, *Macromolecules*, 2012, **45**, 8722–8728.
- I. Keen, A. Yu, H. Cheng, K. S. Jack, T. M. Nicholson, A. K. Whittaker and I. Blakey, *Langmuir*, 2012, **28**, 15876–15888.
- D. P. Sweat, M. Kim, A. K. Schmitt, D. V. Perroni, C. G. Fry, M. K. Mahanthappa and P. Gopalan, *Macromolecules*, 2014, **47**, 6302–6310.
- W. J. Durand, G. Blachut, M. J. Maher, S. Sirard, S. Tein, M. C. Carlson, Y. Asano, S. X. Zhou, A. P. Lane, C. M. Bates, C. J. Ellison and C. G. Willson, *J. Polym. Sci. Part A Polym. Chem.*, 2015, **53**, 344–352.
- C. Sinturel, F. S. Bates and M. A. Hillmyer, *ACS Macro Lett.*, 2015, **4**, 1044–1050.
- T. Seshimo, R. Maeda, R. Odashima, Y. Takenaka, D. Kawana, K. Ohmori and T. Hayakawa, *Sci. Rep.*, 2016, **6**, 4–11.
- G. W. Yang, G. P. Wu, X. Chen, S. Xiong, C. G. Arges, S. Ji, P. F. Nealey, X. B. Lu, D. J. Darensbourg and Z. K. Xu, *Nano Lett.*, 2017, **17**, 1233–1239.
- R. Nakatani, H. Takano, A. Chandra, Y. Yoshimura, L. Wang, Y. Suzuki, Y. Tanaka, R. Maeda, N. Kihara, S. Minegishi, K. Miyagi, Y. Kasahara, H. Sato, Y. Seino, T. Azuma, H. Yokoyama, C. K. Ober and T. Hayakawa, *ACS Appl. Mater. Interfaces*, 2017, **9**, 31266–31278.
- S. H. Kim, M. J. Misner, T. Xu, M. Kimura and T. P. Russell, *Adv. Mater.*, 2004, **16**, 226–231.
- C. M. Bates, T. Seshimo, M. J. Maher, W. J. Durand, J. D. Cushen, L. M. Dean, G. Blachut, C. J. Ellison and C. G. Willson, *Science*, 2012, **338**, 775–779.
- M. J. Maher, C. M. Bates, G. Blachut, S. Sirard, J. L. Self, M. C. Carlson, L. M. Dean, J. D. Cushen, W. J. Durand, C. O.

- Hayes, C. J. Ellison and C. G. Willson, *Chem. Mater.*, 2014, **26**, 1471–1479.
- 26 J. Zhang, M. B. Clark, C. Wu, M. Li, P. Trefonas and P. D. Hustad, *Nano Lett.*, 2016, **16**, 728–735.
- 27 S. Kim, P. F. Nealey and F. S. Bates, *ACS Macro Lett.*, 2012, **1**, 11–14.
- 28 H. Li, W. Gu, L. Li, Y. Zhang, T. P. Russell and E. B. Coughlin, *Macromolecules*, 2013, **46**, 3737–3745.
- 29 S. X. Zhou, D. W. Janes, C. B. Kim, C. G. Willson and C. J. Ellison, *Macromolecules*, 2016, **49**, 8332–8340.
- 30 K. Yoshida, L. Tian, K. Miyagi, A. Yamazaki, H. Mamiya, T. Yamamoto, K. Tajima, T. Isono and T. Satoh, *Macromolecules*, 2018, **51**, 8064–8072.
- 31 P. Mansky, Y. Liu, E. Huang, T. P. Russell and C. Hawker, *Science*, 1997, **275**, 1458–1460.
- 32 P. Mansky, T. P. Russell, C. J. Hawker, J. Mays, D. C. Cook and S. K. Satija, *Phys. Rev. Lett.*, 1997, **79**, 237–240.
- 33 T. P. Russell, R. P. Hjelm, Jr. and P. A. Seeger, *Macromolecules*, 1990, **23**, 890–893.
- 34 Y. Zhao, E. Sivaniah and T. Hashimoto, *Macromolecules*, 2008, **41**, 9948–9951.
- 35 L. Wan, R. Ruiz, H. Gao, K. C. Patel, T. R. Albrecht, J. Yin, J. Kim, Y. Cao and G. Lin, *ACS Nano*, 2015, **9**, 7506–7514.
- 36 G. Hild, J. P. Lamps and P. Rempp, *Polymer*, 1993, **34**, 2875–2882.
- 37 G. Hild and J. P. Lamps, *Polymer*, 1998, **39**, 2637–2649.
- 38 C. E. Hoyle, A. B. Lowe and C. N. Bowman, *Chem. Soc. Rev.*, 2010, **39**, 1355–1387.
- 39 S. De and A. Khan, *Chem. Commun.*, 2012, **48**, 3130–3132.
- 40 S. De, C. Stelzer and A. Khan, *Polym. Chem.*, 2012, **3**, 2342–2345.
- 41 S. Li, J. Han and C. Gao, *Polym. Chem.*, 2013, **4**, 1774–1787.
- 42 E. M. Muzammil, A. Khan and M. C. Stuparu, *RSC Adv.*, 2017, **7**, 55874–55884.
- 43 D. K. Owens and R. C. Wendt, *J. Appl. Polym. Sci.*, 1969, **13**, 1741–1747.
- 44 H. Takano, L. Wang, Y. Tanaka, R. Maeda, N. Kihara, Y. Seino, H. Sato, Y. Kawamozono, K. Miyagi, S. Minegishi, T. Azuma, C. K. Ober and T. Hayakawa, *J. Photopolym. Sci. Technol.*, 2015, **28**, 649–652.
- 45 D. Schrader, in *Polymer Handbook*, ed. J. Brandrup, E. H. Immergut and E. A. Grulke, Wiley-Interscience, New York, 4th ed., 1999, Vol. 1, p V/91.
- 46 R. J. Andrew and E. A. Grulke, in *Polymer Handbook*, ed. J. Brandrup, E. H. Immergut and E. A. Grulke, Wiley-Interscience, New York, 4th ed., 1999, Vol. 1, p VI/211.
- 47 M. W. Matsen and F. S. Bates, *Macromolecules*, 1996, **29**, 1091–1098.
- 48 L. Leibler, *Macromolecules*, 1980, **13**, 1602–1617.
- 49 S. Sakurai, K. Mori, A. Okawara, K. Kimishima and T. Hashimoto, *Macromolecules*, 1992, **25**, 2679–2691.
- 50 N. Sakamoto and T. Hashimoto, *Macromolecules*, 1995, **28**, 6825–6834.
- 51 M. J. Maher, J. L. Self, P. Stasiak, G. Blachut, C. J. Ellison, M. W. Matsen, C. M. Bates and C. G. Willson, *ACS Nano*, 2016, **10**, 10152–10160.
- I. In, Y. H. La, S. M. Park, P. F. Nealey and P. Gopalan, *Langmuir*, 2006, **22**, 7855–7860.
- E. Han, K. O. Stuen, Y. H. La, P. F. Nealey and P. Gopalan, *Macromolecules*, 2008, **41**, 9090–9097.
- S. Wu, *J. Phys., Chem.*, 1970, **74**, 632–638.



79x40mm (600 x 600 DPI)